Polyether Catalysis of Ester Aminolysis – A Computational and Experimental Study

Hendrik Zipse[a]*, Li-hsing Wang[a], and Kendall N. Houk[b]

Institut für Organische Chemie, Technische Universität Berlin[a],
Straße des 17. Juni 135, D-10623 Berlin, Germany
Telefax: (internat.) +49(0)30/3142-1102
E-mail: zips0531@z1.chem.tu-berlin.de

Department of Chemistry and Biochemistry, University of California[b],
Los Angeles, California 9005-1569, USA

Received May 3, 1996

Key Words: Aminolysis / Esters / Catalysis / Calculations, ab initio

Model systems for the reaction of amines with esters were investigated with ab initio methods. Ammonia and methylamine were used as models for primary amines, and formic acid, methyl acetate, phenyl acetate, and *p*-nitrophenyl acetate were chosen to represent typical esters. Geometry optimizations were performed for all systems with the HF/6-31G** method, and relative energies were evaluated by using MP2/6-31G** single-point energies. The lowest barriers are found for the reaction of methylamine with *p*-nitrophenyl acetate. Reaction occurs in this case according to a direct displacement pathway, in which all bond formation and breaking occurs in a single step. Complexation of the transition structures by dimethyl ether or dimethoxyethane leads to much the same changes as observed for variation of the leaving group. Based on the ab initio data a force field for the calculation of transition state-catalyst complexation was developed. This force field as well as ground state complexation energies were employed to predict catalytic activities for a number of polyethers, polyalcohols, and pyrans, which in part, were also investigated experimentally.

The aminolysis of esters has been studied frequently as a model process for the formation of peptide bonds. The mechanism of this reaction has been investigated in detail in water[1a] as well as in a variety of organic solvents[2]. Catalysis of this reaction has attracted considerable attention, due to the attractive goal of selective peptide synthesis. A number of enzymes catalyze the formation of peptide bonds[3,4]. Modified versions of subtilisin have proven especially valuable for synthetic purposes in this respect[5,6,7,8]. Catalytic antibodies have also been found to catalyze the aminolysis of amino acid esters[9,10]. In organic media, the aminolysis of esters is general acid-base catalyzed[1,11]. The aminolysis of adenosine esters with butylamine and aminoadenosine have been studied on a variety of templates by Rebeck et al. in connection with the observation of selfreplication. The catalytic structures used include binding sites for the adenine moiety as well as catalytically active centers[12]. Transition metal Lewis acids have been found to be effective aminolysis catalysts[13]. Polyethers weakly catalyze the reaction of primary amines with phenyl acetates, and the use of structurally different ethers provided some insight into the structure of the transition state of the rate determining step[14]. This latter study employed *p*-nitrophenyl acetate and *n*-butylamine as substrates in chlorobenzene solution. This choice warrants a sufficient reaction rate even in the absence of catalysts as well as easily detectable reaction products. We will therefore use the same system to test the catalytic activities of modified polyethers.

For a reaction as well investigated as the aminolysis of esters, one should assume the development of catalysts to be a straightforward matter, requiring only the design of molecules to afford transition state stabilization[1b]. Following this principle, the recipe for the de novo design of a catalyst could be as follows: (1) Find the lowest energy reaction pathway for the *uncatalyzed* reaction under study. (2) Determine the structure of the highest transition state on this pathway. (3) Design a catalyst that recognizes this transition structure better than any other structure on the pathway. (4) Synthesize the catalyst and study its catalytic properties. Using a combination of quantum mechanical and force field methods, we have set out to test this procedure for the reaction of primary amines with *p*-nitrophenyl acetate.

Ab initio Study of Various Model Systems

Ammonia and Formic Acid

This small model system has been investigated before with ab initio methods[15]. Also, the catalytic effects of H_3O^+, H_2O, and OH^- have been studied for this system[16,17]. Generally, three different reaction pathways should be considered for the uncatalyzed reaction based on earlier studies and on experimental results (Figure 1). The first pathway leads from reactants **1** and **2** to zwitterionic intermediate **6**. Proton transfer from nitrogen to oxygen via transition structure **7** gives the uncharged tetrahedral intermediate **8**. The final products water (**3**) and formamide (**4**)

  0947–3440/96/1010–1511 $ 15.00+.25/0

can be formed from **8** by first transferring a proton between hydroxy groups and then eliminating water from zwitterionic intermediate **10**. This first pathway might best be termed "fully stepwise", since all C–O/C–N bond forming- and breaking steps occur separately and proton transfer is completely uncoupled from these steps. The formation of zwitterionic intermediates such as **6** and **10** can be avoided by merging the C–X bond forming/breaking steps together with the proton transfer processes. The uncharged tetrahedral intermediate **8** is then formed via transition structure **12**, and the final products are obtained via transition structure **13**. This second pathway can best be termed "addition/elimination" pathway, since nucleophilic addition to the C–O double bond first leads to formation of the tetrahedral intermediate and then elimination occurs to regenerate the C=O bond. The third reaction pathway avoids formation of intermediates altogether by cleaving the C–O bond at the same time as the C–N bond is formed. Concomitant proton transfer as in transition structure **14** avoids the formation of charged products. The C–O double bond does not participate in this reaction pathway, which will be termed "direct substitution" pathway.

Figure 1. Possible reaction paths for the reaction of formamide + water to formic acid + ammonia

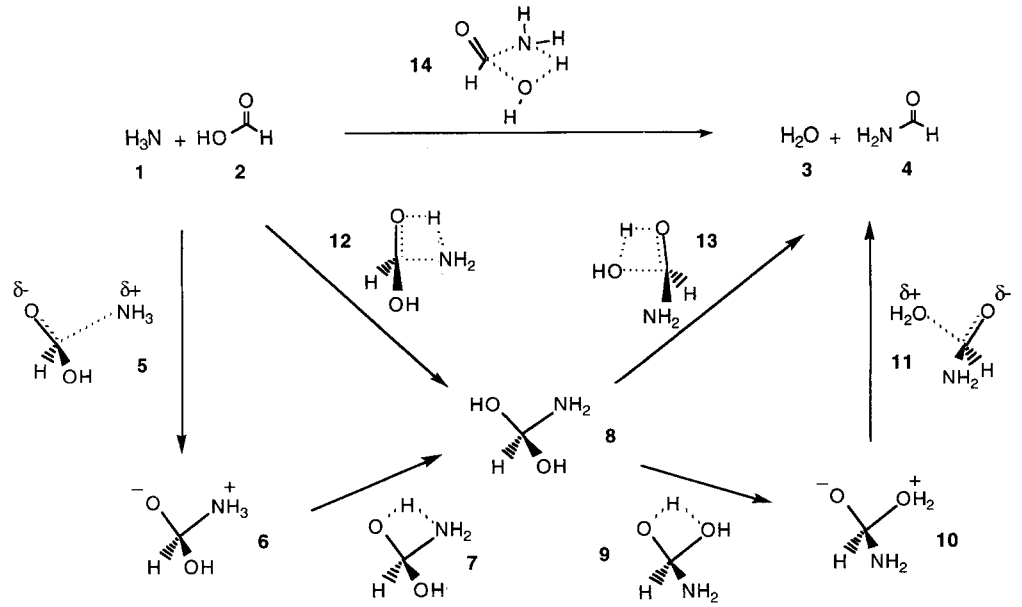

In their earlier computational study, Loew et al.[15] studied the potential energy surface at the ab initio HF/3-21G level and evaluated relative energies by single point calculations at the MP4(FC)/6-31G** level of theory. Only transition states **12** and **13** from the addition/elimination mechanism and transition state **14** from the direct substitution pathway could be found. This was also true at the ab initio HF/STO-3G and the semiempirical MNDO level. It therefore appears that the formation of zwitterionic intermediates like **6** or **10** and the corresponding transition states **5**, **7**, **9**, and **11** are energetically too costly in the gas phase. We have studied this system at the Hartree-Fock level with 3-21G and 6-31G** basis sets and at the correlated MP2/6-31G** level. We tested which theoretical method is suitable for the study of larger model systems and whether zwitterionic intermediates could be found as stationary points with any of these theoretical models[18]. This was not the case at any of these levels; transition structures of rather similar geometry (Figure 2) are obtained in every case. A second conformer exists for **13**, in which the non-transferable water hydrogen atom points away from the formamide nitrogen. Energetically, this structural isomer is at most levels slightly less favorable than **13**. A different conformation is also possible for transition structure **14**, in which the non-transferable water hydrogen atom points away from the carbonyl oxygen atom. This second structure is several kcal/mol less stable than **14** and is not even a stationary point at the HF/3-21G level. Four different conformers of intermediate **8** have been optimized, and the most favorable one is shown in Figure 2.

In general, increasing the basis set from 3-21G to 6-31G** leads to structurally later transition states, while inclusion of electron correlation reverses this trend. Similar compensatory effects of basis set size and treatment of electron correlation have been observed for geometries of ground state molecules before[19]. The effects observed here are, however, not very dramatic. Reaction barriers were calculated from MP2/6-31G** single point energies on geometries calculated at the three different theoretical levels, with zero point energy corrections calculated at the level of geometry optimization. Based on the very similar results obtained at all three levels, we have chosen the combination of MP2/6-31G** energies with HF/6-31G** geometries for the study of all remaining model systems.

The addition/elimination pathway via transition structures **12** and **13** is slightly preferred over the direct substitution pathway via **14**. It is worth noting that the rate limiting step along the addition/elimination pathway consists in

Figure 2. Stationary points in the reaction of ammonia with formic acid; geometries are given at the HF/3-21G, HF/6-31G**, and MP2/6-31G** levels of theory; relative energies are obtained from single point MP2/6-31G** energies, corrected for differences in zero point vibrational energies at the level of geometry optimization

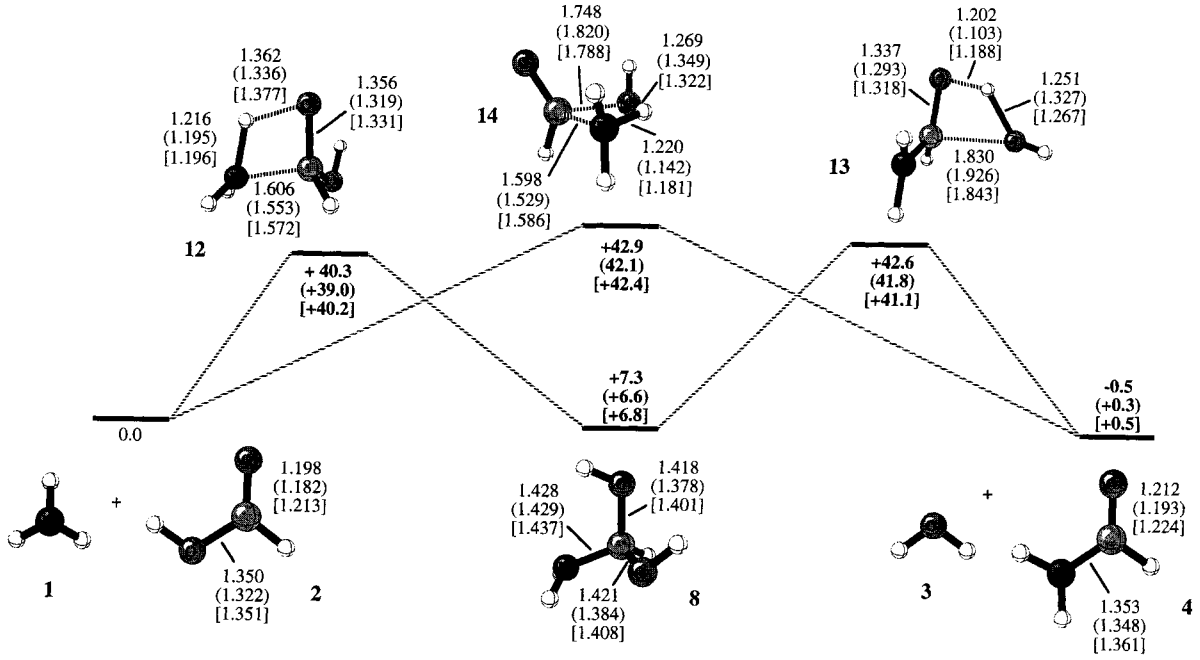

water expulsion from tetrahedral intermediate **8**. Formation of **8** is endothermic by 6–7 kcal/mol, while the overall reaction is essentially thermoneutral.

A Larger Model System: Methylamine and Methyl Acetate

Replacing ammonia with methylamine (**15**) is a significant step toward modeling *n*-butylamine, with respect to size as well as basicity[14]. Methyl acetate (**16**) is used as a simple ester model, which introduces some of the steric bulk in aryl acetates. The ground state geometries of **15** and **16**, two transition state structures **17** and **18** for addition of methylamine to the C=O bond, and transition state structures **19** and **20** for the direct displacement of the methoxy group in methyl acetate have been optimized at the HF/6-31G** level (Figure 3). Structures **17** and **18** differ in the *cis* and *trans* orientations of the two methyl groups. The same is true for structures **19** and **20**. All four structures contain methyl acetate in the *s-cis* conformation. The corresponding *s-trans* structures are higher in energy by at least 5 kcal/mol, if they can be located as stationary points at all. In order to characterize the transition structures **17**–**20** further, atomic charges have been calculated from the HF/6-31G** electrostatic potential (ESP) by using the CHELPG method[20]. The sums of all atomic charges for the methyl amine moieties are included in Figure 3.

The activation barriers for this system (Figure 3) are lower than those calculated for the corresponding structures in the ammonia + formic acid system (Figure 2). The lowest activation barrier for the addition/elimination pathway leading via transition structure **18** is now +35.5 kcal/mol, down from +39.0 kcal/mol in the formic acid/ammonia system. This is the barrier for formation of the tetraheral intermediate alone, and the transition structures for decomposition of the tetrahedral intermediate have not been optimized for this system (see discussion below). An even larger lowering of the activation barrier can be found for the direct substitution pathway via structure **19**, which now has a barrier of +36.2 kcal/mol, down from 42.1 kcal/mol for structure **14**. As a consequence, the two pathways have barriers of similar magnitude in the methylamine/methyl acetate system.

Even though proton transfer occurs concertedly with changes in C–O and C–N bond orders in all structures **17**–**20**, the synchronicity of these processes is quite different in the two pathways. In the addition/elimination transition structures **17** and **18**, the similar magnitude of N–H and H–O bond lengths as well as the low charge separation between methylamine and methyl acetate are indicative of a truly concerted, synchronous addition reaction. This is not so in the direct substitution pathway, in which proton transfer has hardly begun, while C–O bond cleavage and C–N bond formation are almost complete in **19** and **20**. As a consequence, the charge separation in these structures is significantly larger as compared to **17** or **18**. In order to test, whether zwitterionic intermediates are located somewhere on the reaction coordinate, the intrinsic reaction path was followed from structure **19** in forward and backward direction for twenty steps in mass-weighted internal coordinates with a step size of 0.2 au. Selected structures and geometric parameters are shown in Figure 4. The sequence of bond-forming and -breaking in the overall reaction can best be described as follows: Up to the transition state, the methylamine molecule approaches the carbonyl carbon atom, as the methoxy group is cleaved off simultaneously. Proton

Figure 3. Ground and transition states in the reaction of methylamine with methyl acetate optimized at the HF/6-31G** level of theory; activation barriers at the MP2(FC)/6-31G**//HF/6-31G** + ΔZPE level are shown (in kcal/mol); cumulative ESP charges, q(am), obtained from fitting the HF/6-31G** electrostatic potential are given for the methylamine moieties

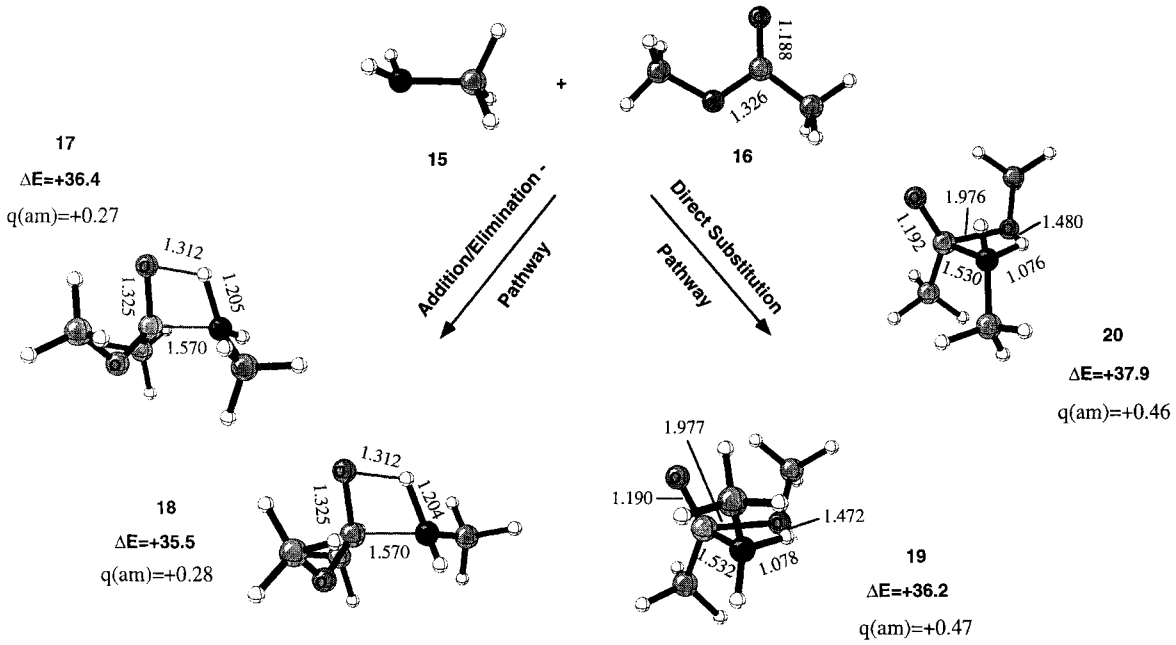

transfer does not occur during this stage. After the reaction passes transition structure **19**, the N–C and C–O bond distances are essentially frozen while proton transfer now occurs for the next 20 kcal/mol down the reaction path. The barrier for this reaction might therefore best be explained by the necessity of creating an electrostatically favorable situation for proton transfer.

Methylamine and Phenyl Acetate

The methylamine + phenyl acetate system differs from the experimental one only by the replacement of *n*-butylamine by methylamine and by omitting the 4-nitro substituent in the phenyl ring.

The preferred conformation of phenyl acetate (**21**) is nonplanar (Figure 5). The planar conformer is a rotational transition state which is only 1.0 kcal/mol higher at the MP2(FC)/6-31G**//HF/6-31G** level. Four transition states **22**–**25** for the reaction of **21** with methylamine have been found (Figure 5). In structures **22** and **23**, addition occurs to the carbonyl double bond to form tetrahedral intermediates. The *trans* orientation of the two methyl groups in **22** is slightly preferred over the *syn* orientation in **23**.

Figure 4. Selected geometric and energetic data from the intrinsic reaction coordinate calculation for the reaction of methylamine with methyl acetate according to the direct displacement pathway; distances are in A and energies in kcal/mol

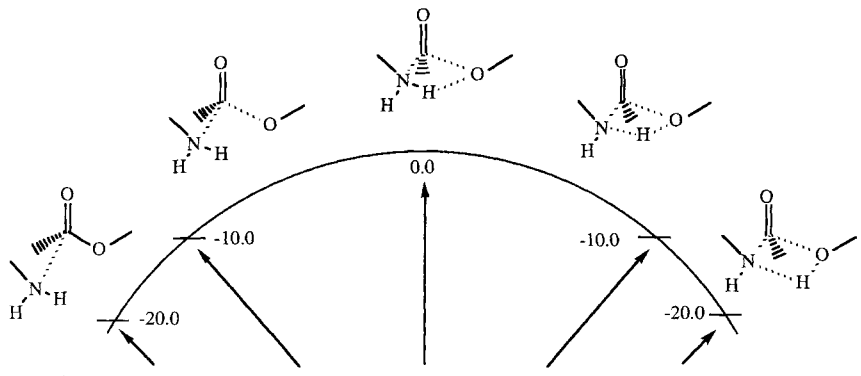

R(C-N) = 1.70	1.61	1.53	1.51	1.50
R(C-O) = 1.52	1.70	1.98	2.02	2.03
R(N-H) = 1.00	1.01	1.08	1.32	1.46

The introduction of the phenyl group lowers the activation barrier by 3.60 kcal/mol. This lower barrier is associated with significant changes in the geometry of the transition structures (Figure 5 vs. 3). Larger changes can be observed for the direct substitution pathway via structures **24** and **25**. The introduction of the phenyl group leads to a lowering of the barrier of ca. 9 kcal/mol. The expulsion of the alkoxide leaving group is more advanced and proton transfer is less advanced in **24** as compared to **19**. Summation of ESP charges over all atomic centers of the amine moiety also shows that charge transfer between amine and acetate is larger for the phenyl-substituted system **24** (+0.55) than for **19** (+0.47). Structure **24** is similar in its electronic and structural properties to the ion pair intermediate proposed by Gandour et al.[14]. Structure **24** might therefore best be termed an "*ion-pair like transition state*". It is important, however, to emphasize that **24** constitutes a unique transition structure and that no ion pair *minimum* has been found along the reaction pathway. The introduction of the *p*-nitro substituent into the phenoxide leaving group is likely to lead to even larger charge separation due to better stabilization of the negative charge, especially in the transition structures of the direct displacement reaction pathway. Transition structure **24** was therefore extended by introduction of a nitro group in the *p* position of the phenyl group and reoptimized (Figure 6).

There is a strong structural resemblance between transition structure **27** for the direct displacement reaction between *p*-nitrophenyl acetate and methylamine and **24**. Introduction of the nitro group causes no major geometrical changes but lowers the activation barrier by almost 10 kcal/mol! Again, the bond distance between the phenoxide oxygen and carbonyl carbon or amine hydrogen suggest an ion-pair like character for this transition structure.

The above results are in accord with the mechanistic analysis of Menger et al., who observed a large dependence of the reaction rate on the leaving group, but little effect of acyl substituents[2]. The cyclic transition structures found here were excluded at that time only because they were thought to imply similar degrees of C–O bond breaking and O–H bond formation. That cyclic transition states do not necessarily have to be synchronous is clearly visible in structures **24** and **27**, both of which are cyclic transition states, but with very different C–O and O–H bond orders.

The high preference for concerted acyl transfer over the addition/elimination mechanism found here is supported by kinetic isotope effects[21a] as well as Brønsted correlations for acyl transfer reactions involving esters with good leaving groups[21b–e]. Computational[22a,b] as well as experimental[22c] gas phase studies of nucleophilic substitution reactions in acyl halides also favor the direct substitution mechanism. The direct displacement transition structures found here might therefore not be as exotic as they appear at first sight.

Variation of Transition Structures in the Presence of Catalytically Active Molecules

The size of the phenyl acetate model system makes the study of additional structural and energetic effects of catalysts impractical. Since it has become clear from the last two model systems that the direct displacement reaction pathway is by far preferred for the uncatalyzed reaction,

Figure 5. Ground and transition states in the reaction of methylamine with phenyl acetate optimized at the HF/6-31G** level of theory; activation barriers ΔE at the MP2(FC)/6-31G**//HF/6-31G** + ΔZPE level are shown (in kcal/mol); charges, *q*(am), refer to cumulative ESP charges for methylamine

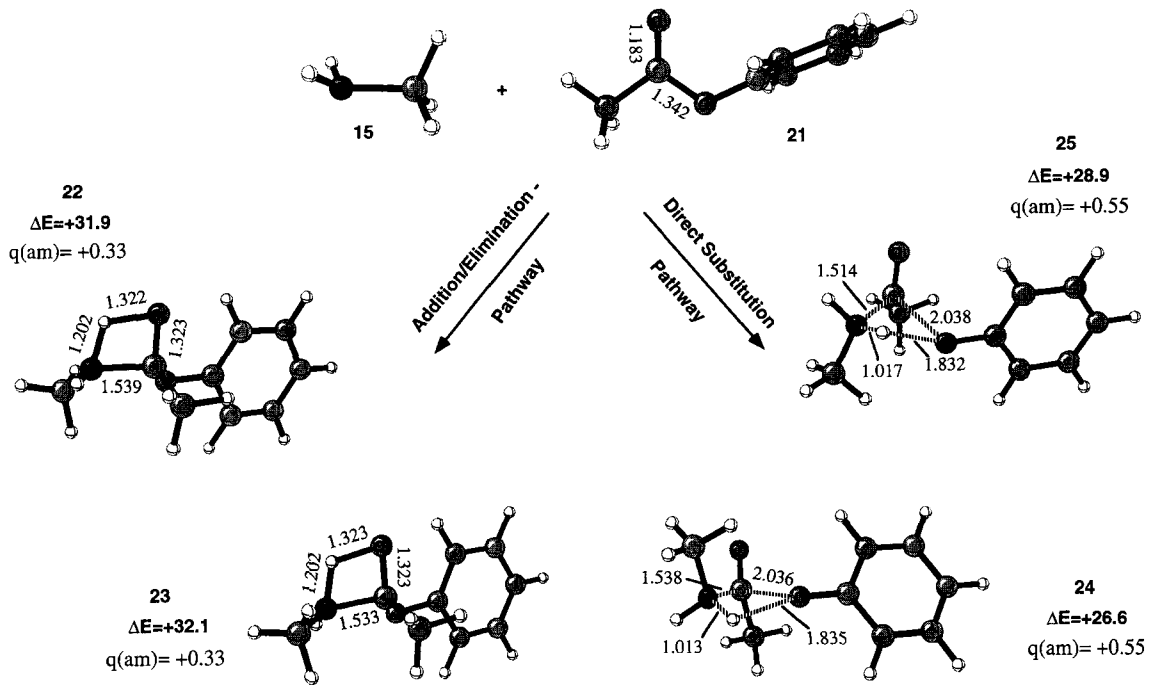

Figure 6. Ground and transition states in the direct displacement reaction of methylamine with *p*-nitrophenyl acetate at the MP2/6-31G**//HF/6-31G** level of theory; the activation barrier is given in kcal/mol and the charge *q*(am) refers to cumulative ESP charges for methylamine

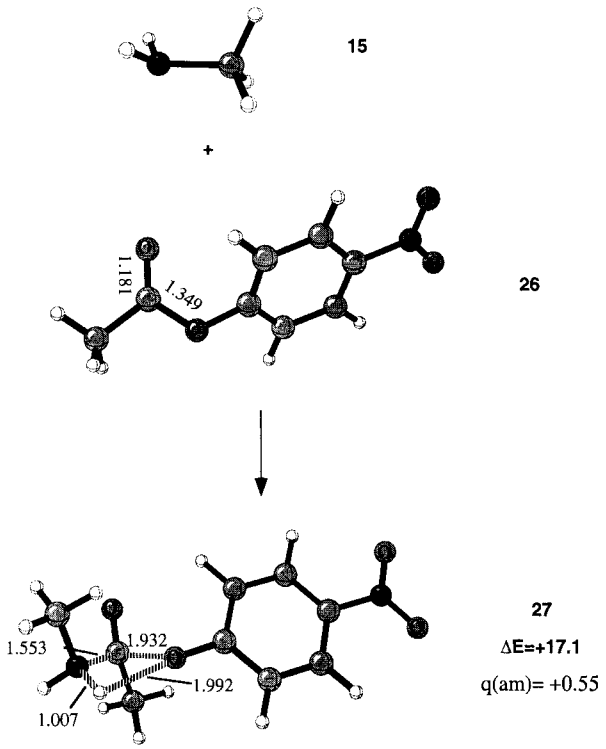

Figure 7. Transition structures for the reaction of methylamine with methyl acetate in the absence and in the presence of ethers (HF/6-31G**)

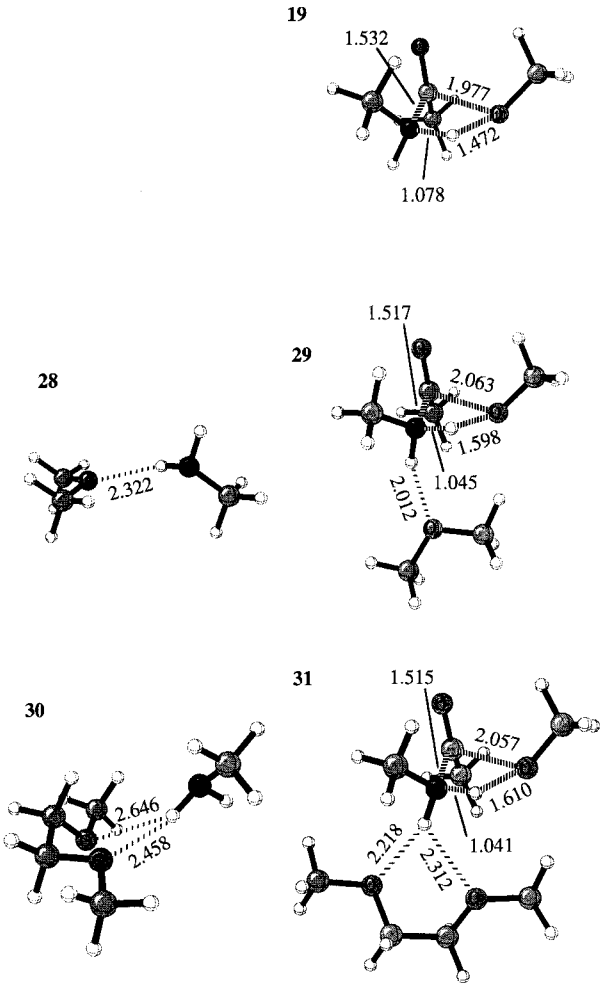

transition structure **19** from the smaller methylamine + methyl acetate system has been used to study the response of transition state structure to the presence of catalysts. Since various polyethers have been used to catalyze this reaction[14], the first catalyst chosen in this study is dimethyl ether.

Dimethyl ether forms only a weak complex with methylamine. The lowest-energy structure of this complex **28** is bound by 3.7 kcal/mol and contains a long N−H···O hydrogen bond. Rotation around this bond is facile and leads to other complexes of almost identical energy. The N−H···O bond is considerably shorter in transition structure **29** than in ground state complex **28** (Figure 7). Dimethyl ether forms a hydrogen bond to the proton *that does not undergo N to O transfer*. Even when the ether was docked to the hydrogen atom in transition structure **19** that undergoes N to O transfer, structure **29** was obtained after geometry optimization. Complexation by dimethyl ether leads to increased N−C bond formation and C−O bond cleavage. Also, hydrogen transfer is far less evolved in **29** as compared to **19**. Overall, the effects of ether complexation are the same as compared to improvement of the leaving group in that both modifications lead to increased zwitterionic character of the transition structures.

Use of the bidentate 1,2-dimethoxyethane (DME) has much the same effect as compared to dimethyl ether. Again, a weak complex **30** is formed with methylamine. Complexation actually occurs with only one of the amine protons, and this proton binds closer to one of the DME oxygen atoms than to the other. In transition structure **31** both ether oxygens complex the amine hydrogen atom that is not undergoing transfer. The geometric changes of transition structure **31** are essentially the same as observed for dimethyl ether.

Figure 8 shows the energetics of the reaction with and without ether catalysts. The stronger hydrogen bonding of ethers to transition structures as compared to the amines translates into strong catalysis. The intrinsic barrier for reaction of methylamine with methyl acetate decreases from +36.1 to +27.4 kcal/mol through catalysis by dimethyl ether. The complexation energy of dimethyl ether is −3.7 kcal/mol with methylamine and −12.4 kcal/mol with transition structure **19**. DME is not a better catalyst as compared to dimethyl ether, because the complexation of the transition structure is about the same, −12.5 kcal/mol, while the methylamine/DME complexation energy is −5.4 kcal/mol.

Figure 8. Variation of the activation barrier in the methylamine + phenyl acetate reaction inclusion of catalytically active ethers (MP2/6-31G**/HF/6-31G** + ΔZPE(HF/6-31G**)) [kcal/mol]

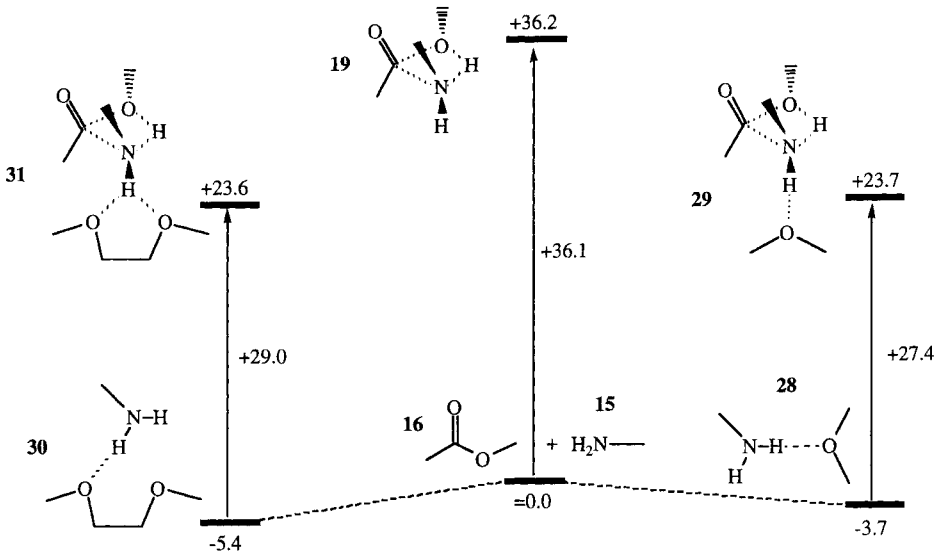

To compare the structural variations caused by catalysis, Pauling bond orders were calculated according to equation (1) for the most favorable transition structures on the direct displacement pathways. Equation (1) relates bond order n_p to a reference bond order n_0 by a factor, which includes the differences in bond lengths of the two structures[23].

$$n_p = n_0 \exp\left\{\frac{R_0 - R_p}{0.6}\right\} \quad (1)$$

Four bond orders are of interest for this reaction. To construct a More O'Ferrall-Jencks diagram, the difference in the two variables describing proton transfer (N–H and O–H bond order) is plotted on the y axes, and the difference between the variables describing acyl transfer (C–N and C–O bond order) is plotted on the x axis. Even though these bond order differences do not describe the transition structures exactly, it allows the description of the overall reaction in a two-dimensional More O'Ferrall-Jencks diagram (Figure 9). All direct displacement transition structures investigated here are located in the lower right half of Figure 9. This is a visual representation of the fact that changes in C–N and C–O bond order far precede proton transfer. Also, the spread of transition structures along the C–O/C–N coordinate is much smaller as compared to that along the N–H/O–H coordinate. In structural terms this implies that the transition structures vary much more in the degree of proton transfer than in acyl transfer. Systematic trends can also be identified for variations in the substrate. Improvement of the leaving group from methoxy to phenoxy or *p*-nitrophenoxy shifts the transition structures mainly downward, that is, transition structures are much earlier in terms of proton transfer. A similar effect can be observed for ether catalysis, which shifts the transition structure from **19** towards the lower right corner. The combined effects of catalysis and a good leaving group will likely shift the transition state further to the lower right corner of Figure 9. Structure **24** is closest to an ion-pair like transition structure and has subsequently been used for molecular modeling.

Merging ab initio and Force Field Data

Studying even larger systems with quantum mechanical methods is not feasible because of the large conformational space which must be investigated. A force field representation of **24** for use with the AMBER force field[24] in its all-atom version as implemented in Batchmin 4.0[25] (AMBER*) was therefore developed. The ab initio structure of transition state **24** was held rigid in all force field calculations, while the structure of the catalyst as well as all intermolecular degrees of freedom were allowed to vary. In order to keep the transition structure fixed to its ab initio geometry, harmonic constraints were added between every atom and its position in space with very high force constants. Distance and angular force field constants were set to values of 800–850 kJ mol^{-1} to reduce the flexibility further. Torsional potentials within substructure **24** were all set to 0.0 kJ mol^{-1}. Parameters for the description of intermolecular interactions were obtained by adopting Lennard-Jones parameters for amides and esters from the literature and by using atom-centered charges derived by fitting the HF/6-31G** electrostatic potential and scaling by a factor of 0.75[20]. Coulomb parameters for the catalyst molecules were taken from the AMBER force field. At the beginning of conformational searches, the transition state structure was manually surrounded by the catalyst. This complex was used as starting point for Monte Carlo searches in which all free torsions, rotations, and movement up to 1 Å of the catalyst molecule was varied within 9000 steps to find the structure of lowest energy. This procedure was repeated for the complex of amine with the glyme catalysts to calculate complexation energies.

Figure 9. More O'Ferrall-Jencks diagram for the aminolysis reaction

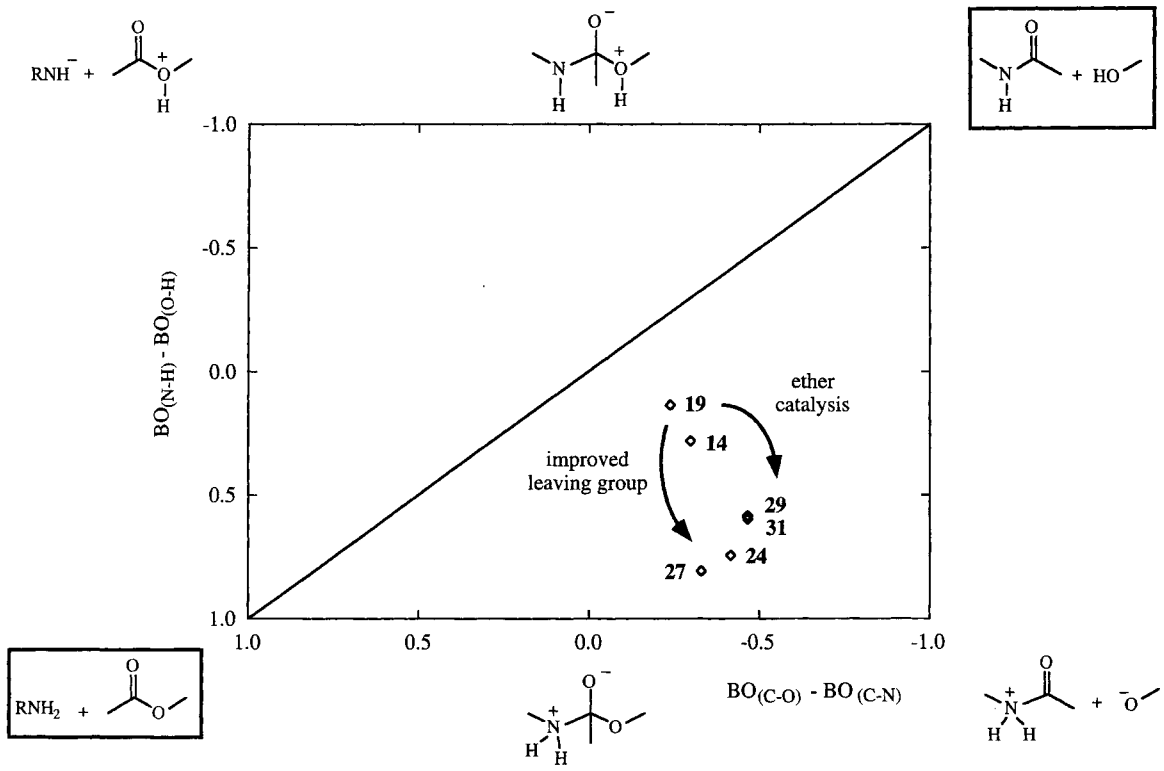

We began by investigating the complex of triglyme (**32**) with transition structure **24** in order to first calibrate our model and then compare to known experimental results. The most favorable complex **33** obtained as described above is shown in Figure 10. The glyme chain wraps around **24** such that each of the amine hydrogen atoms coordinates to two polyether oxygen atoms. According to the H–O distances, the transferred amine hydrogen atom is coordinated less tightly to the polyether chain as compared to the second amine hydrogen atom. Figure 10 also shows schematically two strategies for the improvement of the catalytic activity of polyethers.

1) The flexibility of the free glyme chain is significantly reduced upon binding to the transition structure. Experimentally, this translates into high activation entropies. This problem can be alleviated by freezing the polyether chain in a reactive conformation. The restriction of conformational space is possible for example by integration of the polyether chain into ring systems. In principle, this goal can be achieved by annulation (dashed lines **A** or **B** in Figure 10) or to a C–O–C unit (motive **B**). **A** restricts only one torsional angle, while **B** influences two torsional angles of the polyether chain.

2) While complexation with the glyme chain satisfies the electrostatic requirements of the amine moiety in **24**, no stabilization occurs for centers of negative charge accumulation such as the phenoxide oxygen atom and (to some extend) the carbonyl oxygen atom. Extending polyether catalysts by some functional groups capable of hydrogen

Figure 10. Complex **33** obtained from triglyme (**32**) and transition structure **24**

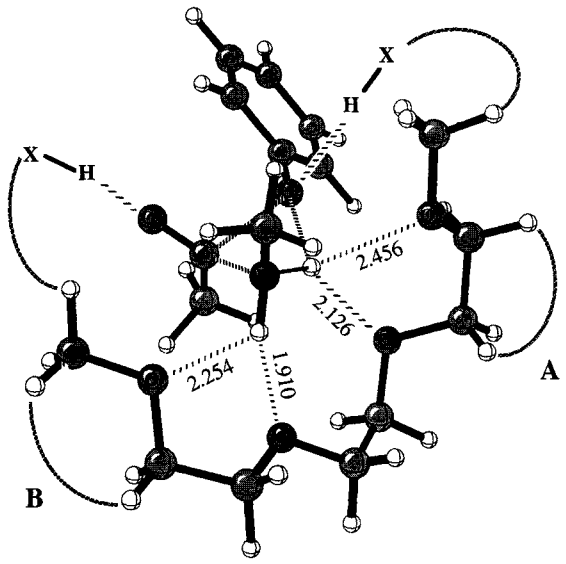

bonding such as shown by the H–X groups in Figure 10 should therefore lead to improved catalytic properties.

3) A third way of altering, perhaps improving, the catalytic potential of glymes consisting in varying the oxygen to oxygen distance along the polyether chain. This can readily be achieved by using O–C–O or O–C–C–C–O instead of O–C–C–O units.

We have experimentally determined catalytic rate constants for a number of modified polyether catalysts, which incorporate one or more of the above three points of improvement. For reference, the catalytic activities of smaller, linear glymes have also been determined experimentally and included in Table 1. Structures of all investigated systems are given in Scheme 1.

Scheme 1

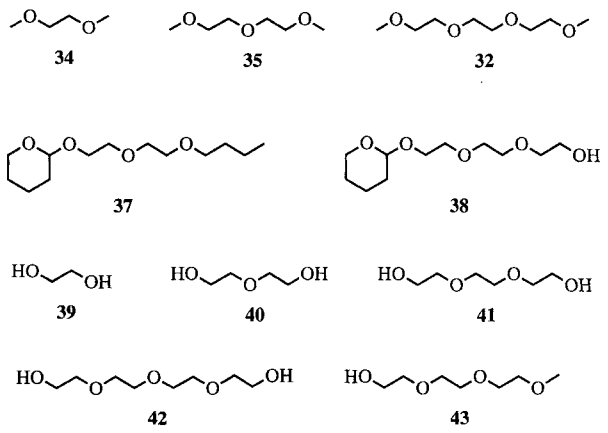

Table 1. Kinetic data for all catalysts investigated in this study

Catalyst	concentration [mmol l^{-1}]	k_{cat} (22°C)[a] [l^2 mol^{-2} s^{-1}]	Δk_{cat}	ΔE_A[b] [kcal mol^{-1}]
32	4.3-21.4	0.320 (0.308)	±3%	-4.0
34	8.2-40.8	0.024 (0.018)	±45%	-2.3
35	5.5-27.4	0.150 (0.174)	±5%	-3.5
18C6 (**36**)	4.1-16.5	0.029 (0.022)	±56%	-
37	7.7-45.9	0.054	±8%	-3.9
38	5.5-27.4	0.112	±5%	-
39	11.0-44.0	0.112[c]	±2.5%	-2.8
40	7.5-22.5	0.244[c]	±6%	-2.3
41	7.2-28.8	0.531	±11%	-2.9
42	4.5-22.3	0.463	±9%	-3.0
43	4.5-24.7	0.430	±8%	-3.8

[a] Values given in parentheses are taken from ref.[14]. – [b] Barrier lowering as calculated with the AMBER* force field (see text). – [c] T range 23–25°C.

The first three entries in Table 1 list catalytic activities for glymes **32**, **34**, and **35**. These are in very good agreement with those measured before[14]. The increasing activity can well be rationalized by the increasing number of hydrogen bonds between glyme oxygen atoms and amine hydrogen atoms in **24**. The low catalytic activity of 18-crown-6 can also easily be rationalized since the ring size of this crown ether does not permit complete binding of **24**. Binding of 18-crown-6 to **24** is, of course, also possible in a side-on mode, but this requires a significant deformation energy of the catalyst. The low activity of **37**, which is less than for **35**, came somewhat as a surprise. Since **37** contains **35** as a substructure extended with a tetrahydropyran ring, a larger catalytic efficiency was expected. The same disappointing result was obtained for **38**. In both cases, this can be due to either O–C–O motives being less catalytically active as compared to O–C–C–O sequences, or to unfavorable conformational properties of the tetrahydropyran substructures. The low efficiency of **38** is especially surprising since all polydiols show higher catalytic activities than the corresponding glymes. This is already visible for ethylene glycol (**39**), which shows catalytic effects identical to **38**. The transition state/ethylene glycol complex shows only one hydrogen bond between the amine hydrogen atom and one of the glycol oxygen atoms. The second oxygen atom is involved in *intramolecular* hydrogen bonding. The same situation is found in the transition structure complex with **41** (Scheme 2).

Scheme 2

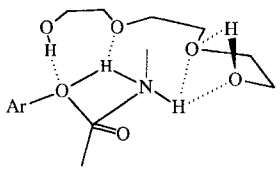

Increasing the chain length even further to **42**, both negatively charged centers of transition structure **24** can be reached as depicted in Figure 10. Surprisingly then, the best catalyst in this series is **41** and not **42** (Table 1). This result cannot be rationalized on the basis of complex **33**. Capping one OH terminus in **41** with a methyl group as in **43** lowers the activity slightly, capping the second OH group has a larger effect. The most important result from Table 1 is, however, that catalysis by polydiols is not even a factor of two better as compared to the corresponding glymes! It must therefore be concluded that the expected catalytic effects of the additional hydrogen bonds as schematically depicted in Figure 10 do not result in the expected significant rate enhancements.

To gain better insight into the structural basis of polyether and polydiol catalysis, we define a numerical model for the activation barrier lowering ΔE_A(cat) caused by these catalysts.

Scheme 3

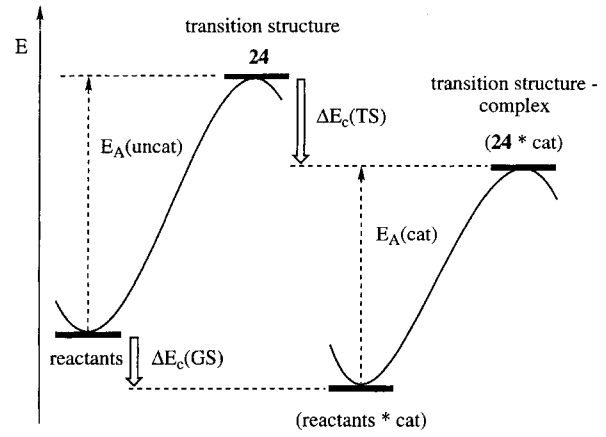

According to Scheme 3, ΔE_A(cat) is given as the difference between the activation barriers of the catalyzed and uncatalyzed reaction, but can also be calculated as the difference between the complexation energy of the ground state ΔE_c(GS) and the complexation energy of the transition structure ΔE_c(TS):

$$\Delta E_A(\text{cat}) = E_A(\text{cat}) - E_A(\text{uncat}) = \Delta E_c(\text{GS}) - \Delta E_c(\text{TS}) \quad (2)$$

The complexation energy of the transition structure **24** ΔE_c(TS) is directly available from our initial investigation of the complexes between **24** and catalysts. We can obtain an estimate of the catalytic potency of catalysts by subtracting the ground state complexation energy. We have used the same methodology as described for the transition state complexes to study complexes between catalysts and methylamine or phenyl acetate. Whatever complex provided the stronger complexation energy was used as the model for the ground state complex. As defined in equation (2), more negative values of ΔE_A(cat) correspond to better catalytic properties. Assuming the activation entropies for catalysis by a family of structurally similar molecules to be comparable, the relative activation energy ΔE_A(cat) should correlate with the relative catalytic rate constant k_{rel} according to equation (3).

$$\Delta E_A(\text{cat}) = 2.3\, RT \log k_{rel} \quad (3)$$

Plotting log k_{rel} vs. ΔE_A(cat) gives a satisfactory correlation for the subgroup of glyme catalysts and a correct prediction of k_{uncat} for $\Delta E_A = 0$ for this group (Figure 11). However, no general correlation between log k_{rel} vs. ΔE_A-(cat) can be seen when all catalysts are included. Unsatisfactory correlations were furthermore obtained with scale factors for Coulomb parameters of 1.00 or 0.50, with and without solvent models, with and without MD conformational sampling, and with ground state complexes consisting of catalysts + amine, catalyst + ester, or catalyst + amine + ester. The low predictive accuracy of our force field model is likely to be due to the small differences in catalytic efficiency of the catalysts used here. Since the accuracy of force fields generally does not exceed ±1 kcal/mol, the correct prediction of small variations in catalytic rate constants is simply not possible. A somewhat better correlation between calculated and experimentally determined data could be found *for all substrates* if only ground state complexation energies were considered (Figure 12). The complexation energy E_{compl} used here is the energy difference between separate reactants and a three-component ground state complex (catalyst + amine + ester). The better predictive value of this latter method is at least in part due to the fact that variations in E_{compl} are more than twice as large as variations in ΔE_A. Also, the ground state model allows a much more flexible relative orientation of the two reactants, while the transition state model employs one fixed transition state geometry for all catalysts.

As a last step in our study, we have used both ΔE_A and E_{compl} to evaluate the catalytic potential of candidates **44**–**47** (Table 2). Structure **44** is composed of a rigid bipyridine backbone and two galactose-derived side chains. The side chains differ in their ability to form hydrogen bonds. The "binding site" of **44** is ideally suited to bind the two reactants, and a very high complexation energy is obtained. The predicted barrier lowering, in contrast, is not much higher than calculated for the glyme catalysts. Structure **45** uses the same side chains, but a much more flexible bridge. This increased flexibility leads to a significantly lower binding energy, but a much better theoretical barrier lowering. Structures **46** and **47** have been conceived as cyclic polyethers, which are (1) large enough to completely bind the transition structure **24** and (2) include amide functionalities oriented such that hydrogen bonds are formed to the carboxylate oxygen atom in **24**. This "oxy-anion hole" motive derived from proteases[1b] is not very successful in this case, however, since neither E_{compl} nor ΔE_A are signficantly different from the values obtained for glymes. The structures obtained for **46** and **47** in the absence of substrate show that the low predicted activity is due to the collapse of the binding site under concomitant formation of hydrogen bonds between amide hydrogen and ether oxygen atoms. Before binding of the substrate, these hydrogen bonds have first to be broken again. Comparing the predicted catalytic potential of compounds **44**–**47**, one has to conclude that *rigidity* appears to be one of the crucial characteristics of

Figure 11. Correlation of the activation energy lowering ΔE_A vs. log k_{cat}

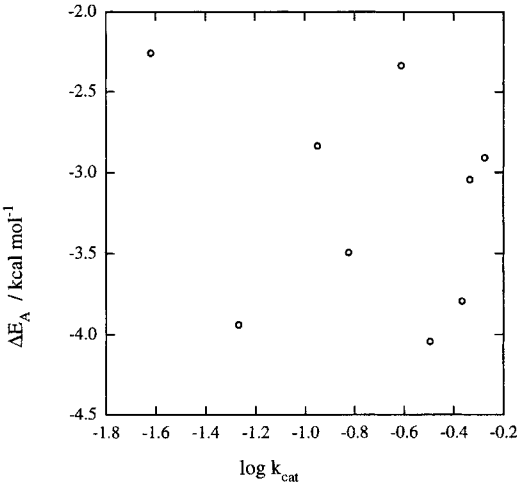

Figure 12. Correlation of complexation energy of the three component ground state complex vs. log k_{cat}

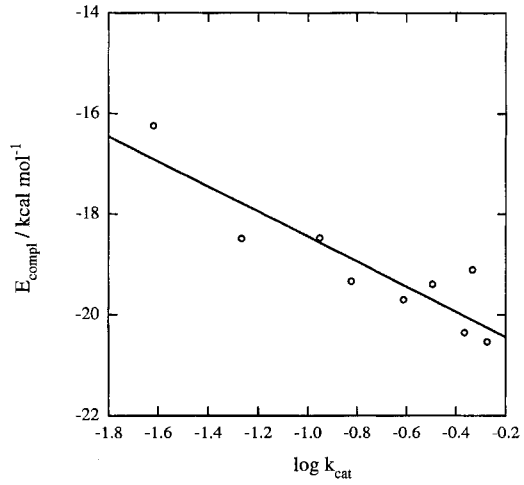

successful catalysts. We are currently investigating different strategies for the synthesis of compounds **44**–**47**.

Table 2. Predicted ground state complexation energies E_{compl} and activation barrier lowering ΔE_A for catalysts **44**–**47**

	E_{compl} [kcal/mol]	ΔE_A [kcal/mol]
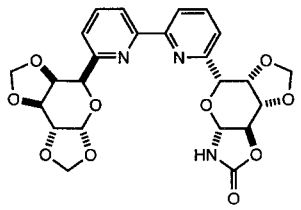 **44**	-29.1	-4.3
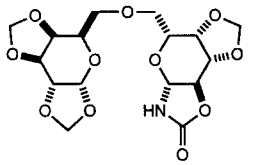 **45**	-24.1	-6.2
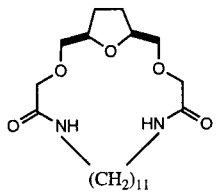 **46**	-20.3	-4.4
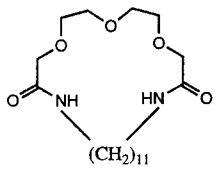 **47**	-21.4	-3.5

Conclusion

The ab initio investigation of several model systems for the reaction of esters with primary amines highlights the importance of single-step, direct displacement pathways. Especially in those models with good leaving groups, the concerted direct displacement pathway has a much lower barrier than the addition/elimination pathway. Complexation of the direct displacement transition structures by simple ethers leads to significantly lower barriers. The most favorable transition structure obtained for the reaction of methylamine with phenyl acetate has been used in combination with force field modeling to elucidate the origin of catalytic activity of polyethers. While the variations in catalytic efficiency of the catalysts investigated here was too small to be reproduced directly with the transition state model, a good correlation was found between catalytic efficiency and theoretically predicted complexation energies between reactants and the catalyst.

This work was supported by the *Deutsche Forschungsgemeinschaft*, the *Fonds der Chemischen Industrie* through a Liebig Stipendium and by Prof. *H. Schwarz* through generous financial support. Computational resources have been provided by the *UCLA Office of Academic Computing*, the *Zentraleinrichtung Rechenzentrum TU Berlin*, and the *Konrad-Zuse-Zentrum für Informationstechnik Berlin*. We thank *S. Ferguson* for some preliminary calculations.

Experimental

Chlorobenzene (Merck), 4-nitrophenyl acetate (Aldrich), glyme (Merck), diglyme, triglyme, triethyleneglycol monomethyl ether, tetraethylene glycol, triethylene glycol, ethylene glycol (Merck), and 18-crown-6 were used as received. *n*-Butylamine was dried with calcium hyride, purified by fractional distillation from calcium hydride and stored under nitrogen for short times only. Diethylene glycol was fractionally distilled under reduced pressure (145–149 °C/40–50 mbar) and fractionally crystallized by partial freezing.

Kinetics: Reactions were carried out by pipetting 2.5 ml of a butylamine/catalyst/chlorobenzene solution (0.117 M in *n*-butylamine) into a 3-ml cuvette, injecting 0.030 ml of a 0.01 M ester/chlorobenzene solution, stoppering and shaking the cuvette and measuring the absorbance of the produced *p*-nitrophenol for about two half-lives at constant wavelength (λ = 320 nm). UV data were measured with a Cary 118c spectralphotometer. Rate constants k_{obs} were obtained by fitting absorbance $A(t)$ versus time data to equation (4) where absorbance after completed reaction A, absorbance before reaction A_0 and k_{obs} are iteratively optimized.

$$A(t) = A_\infty - (A_\infty - A_0) \cdot e^{-k_{obs}t} \quad (4)$$

24 to 48 data points of absorbance $A(t)$ with constant time intervals were used for computational fits. All k_{obs} values were determined by at least three measurements. Kinetic measurements were repeated for a range of different catalyst concentrations (see Table 1). The rate law found for the catalyzed reactions is[14]:

$$k_{obs} = k_A[\text{amine}]^2 + k_{cat}[\text{amine}][\text{catalyst}] \quad (5)$$

Under pseudo-first order conditions, the catalytic rate constants k_{cat} are obtained by plotting k_{obs}/[amine] vs. [catalyst]. The rate constant k_A for the self-catalyzed background reaction was measured as 0.0681 ± 0.02 l^2 mol^{-2} s^{-1}, in good agreement with the literature value of 0.0651[14].

Supplementary Information is Available from the Authors on Request: Eleven (11) pages with structures of all optimized stationary points in Gaussian archive format.

[1] [1a] P. J. Jenks, *Catalysis in Chemistry and Enzymology*, McGraw-Hill, New York, **1969**. – [b] A. R. Fersht, *Enzym Structure and Mechanism*, Freeman, New York, **1985**.
[2] F. N. Menger, J. H. Smith, *J. Am. Chem. Soc.* **1972**, *94*, 3824.
[3] V. Schellenberg, H.-D. Jakubke, *Angew. Chem.* **1991**, *103*, 1440; *Angew. Chem. Int. Ed. Engl.* **1991**, *30*, 1437.
[4] A. L. Margolin, A. M. Klibanov, *J. Am. Chem. Soc.* **1987**, *109*, 3802.
[5] Z.-P. Wu, D. Hilvert, *J. Am. Chem. Soc.* **1989**, *111*, 4513.
[6] [6a] L. Abrahmsen, J. Tom, J. Burnier, K. A. Butcher, A. Kossiakoff, J. A. Wells, *Biochemistry* **1991**, *30*, 4151. – [6b] T. K. Chang, D. Y. Jackson, J. P. Burnier, J. A. Wells, *Proc. Natl. Acad. Sci. USA* **1994**, *91*, 12544. – [6c] D. Y. Jackson, J. P. Burnier, C. Quan, M. Stanley, J. Tom, J. A. Wells, *Science* **1994**, *266*, 243.
[7] C.-H. Wong, M. Schuster, P. Wang, P. Sears, *J. Am. Chem. Soc.* **1993**, *115*, 5893.
[8] T. Nakatsuka, T. Sasaki, E. T. Kaiser, *J. Am. Chem. Soc.* **1987**, *109*, 3808.
[9] J. Guo, W. Huang, T. S. Scanlan, *J. Am. Chem. Soc.* **1994**, *116*, 6062.

[11] [11a] R. Hirschmann, A. B. Smith III, C. M. Taylor, P. A. Benkovic, S. D. Taylor, K. M. Yager, P. A. Sprengeler, S. J. Benkovic, *Science* **1994**, *265*, 234. – [11b] A. B. Smith III, C. M. Taylor, S. J. Benkovic, R. Hirschmann, *Tetrahedron Lett.* **1994**, *35*, 6853. – [11c] C. Su, J. W. Wastson, *J. Am. Chem. Soc.* **1974**, *96*, 1854.

[12] [12a] I. Huc, R. J. Pieters, J. Rebek, Jr., *J. Am. Chem. soc.* **1994**, *116*, 10293. – [12b] R. J. Pieters, I. Huc, J. Rebek, Jr., *Chem. Eur. J.* **1995**, *1*, 183.

[13] T. Yokamatsu, A. Arakawa, S. Shibuya, *J. Org. Chem.* **1994**, *59*, 3506.

[14] [14a] R. D. Gandour, D. A. Walker, A. Nayak, G. R. Newkome, *J. Am. Chem. Soc.* **1978**, *100*, 3608. – [14b] J. C. Hogan, R. D. Gandour, *J. Org. Chem.* **1991**, *56*, 2821. – [14c] J. C. Hogan, R. D. Gandour, *J. Org. Chem.* **1992**, *57*, 55.

[15] T. Oie, G. H. Loew, S. K. Burt, J. S. Binkley, R. D. MacElroy, *J. Am. Chem.Soc.* **1982**, *104*, 6169.

[16] J. P. Krug, P. L. A. Popelier, R. F. W. Bader, *J. Phys. Chem.* **1992**, *96*, 7604.

[17] S. Antonczak, M. F. Ruiz-Lopez, J. L. Rivail, *J. Am. Chem. Soc.* **1994**, *116*, 3912.

[18] M. J. Frisch, M. Head-Gordon, G. W. Trucks, J. B. Foresman, H. B. Schlegel, K. Raghavachri, M. A. Robb, J. S. Binkley, C. Gonzalez, D. J. DeFrees, D. J. Fox, R. A. Whiteside, R. Seeger, C. F. Melius, J. Baker, R. L. Martin, L. R. Kahn, J. J. P. Stewart, S. Topiol, J. A. Pople, *GAUSSIAN 92 dft*, Gaussian Inc., Pittsburgh, PA, **1994**.

[19] W. J. Hehre, L. Radon, P. v. R. Schleyer, J. A. Pople, *Ab initio Molecular Orbital Theory*, Wiley & Sons, New York, **1986**.

[20] C. M. Breneman, K. B. Wiberg, *J. Comp. Chem.* **1990**, *11*, 361–373.

[21] [21a] A. C. Hengge, R. A. Hess, *J. Am. Chem. Soc.* **1994**, *116*, 11256. – [21b] S. Ba-Saif, A. K. Luthra, A. Williams, *J. Am. Chem. Soc.* **1987**, *109*, 6362. – [21c] S. Ba-Saif, A. K. Luthra, A. Williams, *J. Am. Chem. Soc.* **1989**, *111*, 2647. – [21d] P. J: Guthrie, *J. Am. Chem. Soc.* **1991**, *113*, 3941. – [21e] D. Stefanidis, S. Cho, S. Dhe-Paganon, W. P. Jencks, *J. Am. Chem.Soc.* **1993**, *115*, 1650.

[22] [22a] J. F. Blake, W. L. Jorgensen, *J. Am. Chem. Soc.* **1978**, *100*, 3861. – [22b] S. Yamabe, T. Minato, *J. Org. Chem.* **1983**, *48*, 2972. – [22c] O. I. Asubijo, J. I. Brauman, *J. Am. Chem. Soc.* **1979**, *101*, 3715.

[23] K. N. Houk, J. Gonzalez, Y. Li, *Acc. Chem. Res.* **1995**, *28*, 81.

[24] [24a] J. S. Weiner, P. A. Kollman, D. A. Case, U. C. Singh, C. Ghio, G. Alangona, S. Profeta, P. J. Weiner, *J. Am. Chem. Soc.* **1984**, *106*, 765. – [24b] M. Billeter, A. E. Howard, P. A. Kollman, I. D. Kuntz, *J. Am. Chem. Soc.* **1988**, *110*, 8385.

[25] *Batchmin,* Version 4.0, Columbia University, **1993**.

[96117]